



Article

# Wrinkling of Toroidal Shells in Free Hydroforming

Xiaobin Liu <sup>1,2</sup>, Jian Zhang <sup>1,\*</sup> , Ming Zhan <sup>1,\*</sup>, Xilu Zhao <sup>3</sup> , Wenwei Wu <sup>4</sup> and Kaiwei Xu <sup>4</sup>

<sup>1</sup> School of Mechanical Engineering, Jiangsu University of Science and Technology, Zhenjiang 212003, China

<sup>2</sup> Ocean College, Zhejiang University, Zhoushan 316000, China

<sup>3</sup> College of Mechanical Engineering, Saitama Institute of Technology, Saitama 3690293, Japan

<sup>4</sup> China Ship Scientific Research Center, Wuxi 214082, China

\* Correspondence: zhjian127@just.edu.cn (J.Z.); zhanming@just.edu.cn (M.Z.)

**Abstract:** In this study, we investigated toroidal shell wrinkling in free hydroforming. We specifically focused on toroidal shells with a regular hexagonal cross-section. Membrane theory was used to examine the distribution of stress and yield load in both preform and toroidal shells. The wrinkling moment was then predicted using an empirical formula of shell buckling. In addition, the wrinkling state was investigated using a general statics method, and the free hydroforming of toroidal shells was simulated using the Riks method. Subsequently, nonlinear buckling and equilibrium paths were analyzed. A toroidal preform was manufactured, and free hydroforming experiments were conducted. Overall, the experimental results confirmed the accuracy of the theoretical predictions and numerical simulations. This indicates that the prediction method used in the study was effective. We also found that wrinkling occurs during hydroforming in the inner region of toroidal shells due to compressive stress. Consequently, we improved the structure of the toroidal shells and performed analytical calculations and numerical simulations for the analysis. Our results indicate that wrinkling can be eliminated by increasing the number of segments on the inner side of toroidal preforms, thereby improving the quality of toroidal shells.

**Keywords:** wrinkling; toroidal shell; free hydroforming; buckling



**Citation:** Liu, X.; Zhang, J.; Zhan, M.; Zhao, X.; Wu, W.; Xu, K. Wrinkling of Toroidal Shells in Free Hydroforming. *J. Mar. Sci. Eng.* **2024**, *12*, 89. <https://doi.org/10.3390/jmse12010089>

Academic Editor: Carlos Guedes Soares

Received: 2 December 2023

Revised: 26 December 2023

Accepted: 28 December 2023

Published: 1 January 2024



**Copyright:** © 2024 by the authors. Licensee MDPI, Basel, Switzerland. This article is an open access article distributed under the terms and conditions of the Creative Commons Attribution (CC BY) license (<https://creativecommons.org/licenses/by/4.0/>).

## 1. Introduction

Free hydroforming is a popular technology that is widely used for the manufacturing of shell-formed structures because of its ease of operation, cost-effectiveness, and manufacturing flexibility. Wang [1,2] introduced hydroforming technology for shells and successfully produced spherical shells. Yuan [3] further expanded upon this technology. Zhang and his co-researchers [4] achieved the formation of spherical shells through hydroforming technology using various preformed structures. Some scholars [5,6] went a step further, successfully producing a double-layer spherical shell. Zhang and his co-researchers [7] obtained ellipsoidal shells through hydroforming and studied factors such as deformation and stress. Zeng and his co-researchers [8] conducted numerical simulations on the hydroforming of ellipsoidal shells. Some scholars [9,10] have also applied this technology to the manufacturing of pipelines. The research of the above scholars indicates the feasibility of applying hydroforming technology to various types of shell forming. During the free hydroforming of shells, wrinkling and cracking often occur, seriously affecting the quality of forming. Therefore, researchers have always been searching for an effective method to avoid such defects. Liu and his colleagues comprehensively compared existing wrinkling prediction methods and proposed a hybrid method for predicting wrinkling in thin-walled plastic forming [11]. Therefore, establishing a systematic method to predict the occurrence and condition of wrinkles will play a crucial role in optimizing the shell structure, thereby improving the quality of forming.

Toroidal shells are central, symmetric structures with a positive Gaussian curvature, a negative Gaussian curvature, and a zero Gaussian curvature [12,13]. Toroidal shells can be

used as liquid containers [14], underwater pipeline connectors [15], or as pressure hulls for deep-sea equipment [16]. During free hydroforming, toroidal shell deformation is regarded as a complex process. In this process, if wrinkling occurs as an unstable phenomenon, it will directly affect the geometric accuracy and mechanical properties of the formed shell. Meanwhile, this complex deformation behavior renders the accurate prediction and control of wrinkling phenomena difficult. Serving as a basis for the formation of multi-curvature shells, the free hydroforming of toroidal shells is an effective manufacturing technique for processing and forming such shells and metal structures. Adjustment of the structural parameters of toroidal shells plays a major role in ensuring high-quality hydroforming.

Many studies have been conducted to address the problem of wrinkling during shell hydroforming. Zhang and his co-researchers [17] examined the overall hydroforming of single-curvature oblate spheroidal shells. They reported that the circumferential compressive stress observed in the equatorial zone of the shells resulted in wrinkling. They also indicated that wrinkling was eliminated by restricting axial deformation. Yuan and his co-researchers [18,19] used elastic–plastic stability theory to establish the optimal conditions for wrinkling. They proposed the concept of beneficial wrinkles and dead wrinkles in the context of hydroforming. They defined beneficial wrinkles as wrinkles that can be eliminated in subsequent forming stages without having any negative effects on the final product. By contrast, they defined dead wrinkles as wrinkles that are difficult to remove and can adversely affect the quality of the formed shell. Liu and his co-researchers [20,21] investigated the hydroforming process of curved surface shells. They reported that pre-bulging had a positive effect on strain hardening, resulting in improved wrinkling control during the forming process. Chen and his co-researchers [22,23] proposed an analytical model for suppressing the wrinkling of curved shells during hydroforming. They investigated the impacts of various parameters on wrinkling and found that employing an optimal hydroforming pressure facilitates the creation of shells without wrinkles. Moreover, their findings indicate that the sheet metal hydroforming process is effective for effectively suppressing wrinkling.

The finite element method is a commonly used method for studying the deformation of plates and shells. Rezaiee-Pajand and his co-researchers [24–26] developed an efficient triangular shell element and conducted a geometric nonlinear analysis on the shell structure, which proved the ability and accuracy of the element. The research results can improve the structural optimization method and provide new ideas for this study. Kawka and his co-researchers [27] simulated the wrinkling of conical shells using both dynamic and static finite element programs, and the results showed that the initial shape of the finite element mesh affects the results of wrinkling simulation. Yuan and his co-researchers [28] conducted a finite element simulation to examine the hydroforming process of toroidal shells. They investigated the distribution of stress and strain during the hydroforming process and discussed the factors contributing to wrinkling. Teng and his co-researchers [29,30] conducted theoretical, numerical, and experimental studies on the hydroforming process of toroidal shells with different initial structures. They reported that the primary cause of wrinkling is the occurrence of large compressive circumferential strain in subshells of the toroidal shells under external pressure. They also compared the hydroforming of hexagonal shells and octagonal shells and discovered that toroidal shells with an octagonal cross-section exhibited no wrinkles. In conclusion, they reported that the selection of an appropriate initial structure is key to ensuring the quality of toroidal shells. Notably, no study has provided a comprehensive set of methods for accurately predicting and effectively preventing wrinkling in hydroforming. Therefore, further research is required to develop systematic approaches that can be used to reliably predict and mitigate wrinkling problems.

In this study, we investigated toroidal shell wrinkling in the context of free hydroforming. We established a wrinkle prediction method and proposed an improvement plan for toroidal shell structures to eliminate wrinkles. First, the underlying cause of wrinkling was predicted and analyzed through membrane theory and an external pressure buckling formula. Second, numerical simulations were conducted to determine the wrinkling state

and compare it with theoretical results. Third, a toroidal shell was manufactured for a free hydroforming experiment to verify the theoretical and numerical results. Fourth, a solution for wrinkling was proposed, and its feasibility was verified. Overall, the analysis of the mechanics of the wrinkling process and the optimization of preform structures can assist with minimizing or even eliminating wrinkles, ultimately improving the quality of hydroformed toroidal shells. The established prediction method for the wrinkling of hydroformed toroidal shells can provide a reference for engineering structure optimization and reduce the optimization costs.

## 2. Problem Definition

In this study, we investigated a toroidal shell with a hexagonal cross-section. This type of toroidal shell has both cylinders and cones, and its structure is symmetrical from top to bottom. The cylinders and cones can be considered part of the toroidal shell after hydroforming. Meanwhile, when compared to toroidal shells of other shapes, toroidal shells with a hexagonal section are easier to cut and manufacture. We assumed that each point on the cross-sectional boundary of the toroidal shell moved radially to its circumscribed circle during the hydroforming process. As shown in Figure 1, the inner and outer sides of the toroidal preform were composed of two sets of cones and a single set of cylinders, respectively. The toroidal preform had a rotating radius  $R_0$ , a uniform thickness  $t$ , and a target toroidal shell cross-sectional radius  $r_0$ . Table 1 lists the detailed geometric dimensions of the toroidal preform. Notably, the thicknesses listed in the table are average values that were actually measured for the toroidal preform.

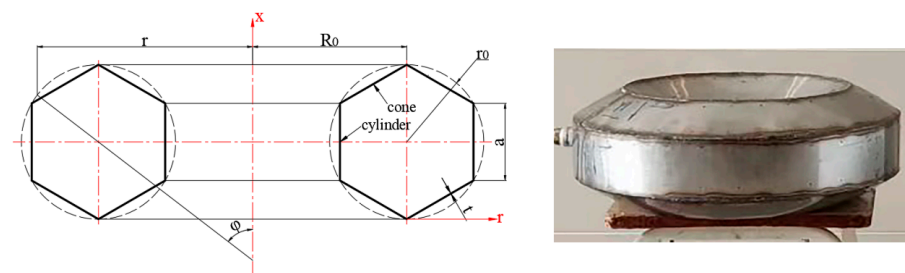


**Figure 1.** Geometry and photograph of a toroidal preform with a hexagonal cross-section.

**Table 1.** Geometric dimensions of the toroidal preform and its target toroid.

$R_0/\text{mm}$	$r_0/\text{mm}$	$a/\text{mm}$	$t/\text{mm}$
150	75	75	1.051

The toroidal preform was fabricated using 304 stainless steel, with the base metal obtained from remaining material in a previous study [31]. Tensile tests were conducted on three tensile specimens to determine the material properties. As shown in Figure 2, the true stress–strain curves obtained were bilinear. Table 2 lists the specific material properties.

To evaluate the wrinkling behavior during the hydroforming process, a mechanical analysis of both the entire toroidal shell and regions with a negative Gaussian curvature was performed using an analytical technique. This analysis was conducted to evaluate the development and state of wrinkling. To gain further insight into the hydroforming process and observe the wrinkling phenomenon, we employed a nonlinear finite element method. This method facilitated the simulation of the toroidal shell hydroforming process and enabled the close observation of the wrinkling process. The results of these analyses, including those of wrinkling and simulations, are presented and discussed in the following section.

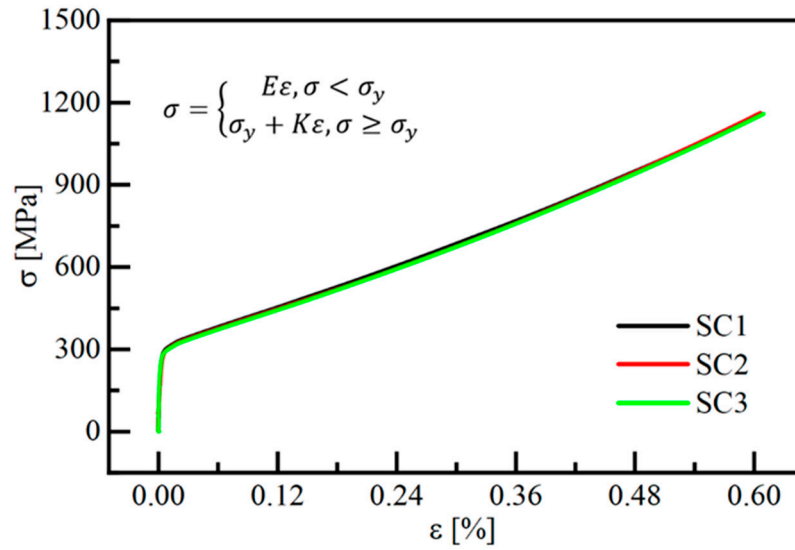


Figure 2. True stress–strain curves of parent material obtained from a uniaxial tensile test.

Table 2. Material properties determined from a uniaxial tensile test.

Sample	E/GPa	$\mu$	$\sigma_y$ /MPa	K/MPa
SC1	191.7	0.29	265	1469.8
SC2	197.5	0.30	252	1405.8
SC3	192.9	0.30	267	1443.3
AVE	194.1	0.30	261	1439.6

E = Young’s modulus;  $\mu$  = Poisson’s ratio;  $\sigma_y$  = yield strength; K = strength coefficient.

### 3. Analytical Studies

As described in this section, membrane theory and a buckling formula were used for a preliminary assessment of the hydroforming process and the underlying cause of wrinkling in toroidal shells.

#### 3.1. Membrane Theory

Let us assume an entire toroidal shell under internal pressure. As shown in Figure 1,  $r$  is the distance from any point on the toroidal shell to the axis of rotation. According to references [2,3], the circumferential stress  $\sigma_\theta$  and meridional stress  $\sigma_\phi$  at each point on the toroidal shell with a target circle can be determined as follows:

$$\sigma_\theta = \frac{pr_0}{2t}, \tag{1}$$

$$\sigma_\phi = \frac{pr_0(r + R_0)}{2rt}. \tag{2}$$

As indicated by Equation (1), the circumferential stress of the toroidal shell is constant. To clearly express the stress distribution of the toroidal shell, the aforementioned equations are integrated to obtain the equivalent stress  $\sigma_e$  as follows:

$$\sigma_e = \sqrt{\sigma_\theta^2 + \sigma_\phi^2 - \sigma_\theta\sigma_\phi}. \tag{3}$$

To obtain the yield load  $p_y$  of the toroidal shell, the equivalent stress  $\sigma_e$  can be equalized to the yield strength  $\sigma_y$  of the material as follows:

$$p_y = \frac{2\sigma_y tr}{r_0\sqrt{r^2 + R_0^2 + rR_0}}. \tag{4}$$



The toroidal preform contains cylinders and cones. According to membrane theory [32], corresponding formulas are used to calculate the membrane stress. The circumferential stress  $\sigma_{\theta\text{-cylinder}}$  and meridional stress  $\sigma_{\varphi\text{-cylinder}}$  of each cylinder are calculated as follows:

$$\sigma_{\theta\text{-cylinder}} = \frac{pr_1}{t}, \tag{5}$$

$$\sigma_{\varphi\text{-cylinder}} = \frac{pr_1}{2t}, \tag{6}$$

where  $r_1$  is the middle radius of the cylinder. The equivalent stress  $\sigma_{e\text{-cylinder}}$  of the cylinder is calculated using Equation (3). Let the equivalent stress  $\sigma_{e\text{-cylinder}}$  be equal to the yield strength  $\sigma_y$ . The yield load  $p_{y\text{-cylinder}}$  of the cylinder is calculated as follows:

$$p_{y\text{-cylinder}} = \frac{2}{\sqrt{3}} \cdot \frac{\sigma_y t}{r_1}. \tag{7}$$

The circumferential stress  $\sigma_{\theta\text{-cone}}$  and meridional stress  $\sigma_{\varphi\text{-cone}}$  of each cone are calculated as follows:

$$\sigma_{\theta\text{-cone}} = \frac{pr_2}{t} \cdot \frac{1}{\cos \alpha}, \tag{8}$$

$$\sigma_{\varphi\text{-cone}} = \frac{pr_2}{2t} \cdot \frac{1}{\cos \alpha}, \tag{9}$$

where  $\alpha$  is the half-cone angle and  $r_2$  is the middle radius of the cone. The equivalent stress  $\sigma_{e\text{-cone}}$  of the cone is calculated using Equation (3). Let the equivalent stress  $\sigma_{e\text{-cone}}$  be equal to the yield strength  $\sigma_y$ . The yield load  $p_{y\text{-cone}}$  of the cone is calculated as follows:

$$p_{y\text{-cone}} = \frac{2}{\sqrt{3}} \cdot \frac{\sigma_y t \cos \alpha}{r_2}. \tag{10}$$

As shown in Figure 3, if the working pressure is  $p = 1$  MPa, then the equivalent stress distribution of an optimal toroidal shell and its preform can be obtained by combining Equations (1) and (3), (5) and (6), and (8) and (9). In this scenario, the overall equivalent stress of the preform is larger than that of the toroid. In addition, the equivalent stress of the outer preform is larger than that of the inner preform. However, this relationship is reversed for the toroidal shell. This behavior arises because of the continuity of the shell's cross-section. Due to the discontinuity of the preform's cross-section, a sudden change in stress occurs at the weld position. Moreover, on the inner cylinder, the equivalent stress of the preform is lower than that of the toroid. Consequently, the deformation that occurs in the inner cylinder during hydroforming is distinct from that in other regions, resulting in a more complex forming process. During hydroforming, the preform is subjected to tensile stress as a whole. The equivalent stress of the cylinder on the inner preform is lower than that of the toroid, indicating the presence of compressive stress. This compressive stress may contribute to wrinkling, a phenomenon associated with the formation of undesirable surface distortions or wrinkles in the material.

As shown in Figure 4, the yield load distribution of a toroidal preform and optimal toroidal shell can be obtained using Equations (4), (7), and (10). This distribution is the opposite of that depicted in Figure 3. In the majority of cases, the yield load of an optimal toroidal shell is larger than that of a preform, indicating that preforms can be transformed into optimal shells through the application of internal pressure. Additionally, the yield load on the inner side of a cylindrical shell is greater than that on an optimal toroidal shell, indicating that an inner cylindrical shell is difficult to form during the hydroforming process. Given the aforementioned phenomenon, the presence of wrinkles in an inner cylindrical shell makes the shell more compressive. Wrinkling induces a longitudinal corrugated shape in cylindrical shells, which has been confirmed by multiple studies [33,34]. In addition, cylindrical shells have superior buckling characteristics relative to similar shells with a negative Gaussian curvature.

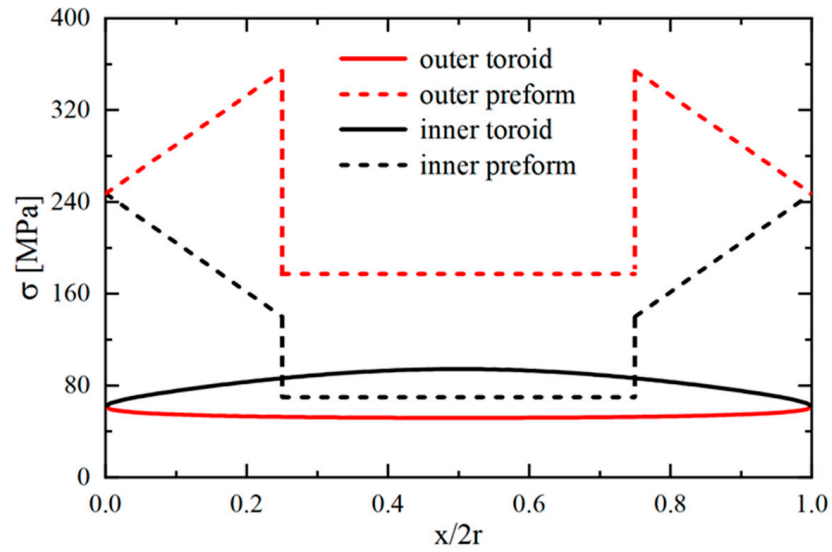


Figure 3. Analytical equivalent stress profile of a toroidal preform and toroidal shell.

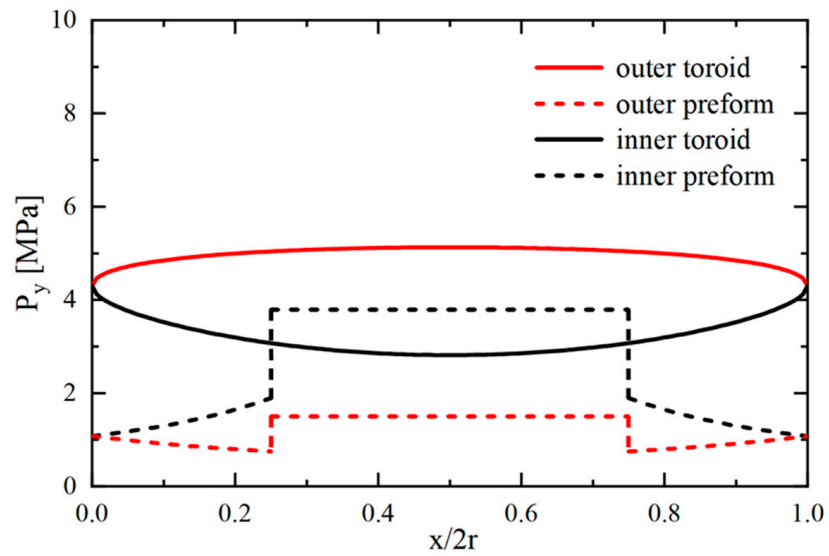


Figure 4. Analytical yield load profile of a toroidal preform and toroidal shell.

### 3.2. Buckling Formula

In a toroidal shell with a negative Gaussian curvature, this region can be considered to bear external pressure during the hydroforming process. To evaluate the wrinkling state in more detail, two buckling formulas were used for the evaluation: Formula (1), proposed by Kollar [30], and Formula (2), proposed by Ventsel and Krauthammer [32]. For computational convenience, we standardized the physical quantities in the two formulas. These formulas have been previously validated and found to yield slightly conservative yet reasonable estimates for shell buckling [35].

In Formula (1), the critical buckling pressure of the cylinder is calculated as

$$p_{cr-cylinder} = \frac{2.59Et^2}{Ld\sqrt{\frac{d}{t}}}, \tag{11}$$

and the critical buckling pressure of the cone is calculated as

$$p_{cr-cone} = \frac{2.6E\left(\frac{t\cos\alpha}{D}\right)^{2.5}}{\frac{l}{D}}. \tag{12}$$

In Formula (2), the critical buckling pressure of the cylinder is calculated as

$$p_{cr-cylinder} = 0.92 \frac{2Et^2}{dL} \cdot \sqrt{\frac{2t}{d}}, \tag{13}$$

and the critical buckling pressure of the cone is calculated as

$$p_{cr-cone} = 0.92 \frac{Et}{l \cos \alpha} \left( \frac{t}{r_m} \right)^{1.5} (\cos \alpha)^{1.5}. \tag{14}$$

In Equations (11)–(14),  $E$  is Young’s modulus,  $t$  is the wall thickness,  $L$  is the cylinder length,  $d$  is the cylinder diameter,  $l$  is the meridian length of the cone,  $D$  is the large-end diameter of the cone, and  $\alpha$  is the half-cone angle.

In particular,  $r_m$  is calculated as follows:

$$r_m = \frac{r_1 + r_2}{2}, \tag{15}$$

where  $r_1$  is the small-end radius of the cone and  $r_2$  is the large-end radius of the cone.

Overall, the data used in the calculation of the aforementioned formulas are derived from those presented in Figure 1 and Table 1. As such, the critical buckling pressure of the inner cylinder and cone can be calculated using the aforementioned formulas. As shown in Table 3, the critical buckling pressure of the cone is less than that of the cylinder, and the critical buckling pressure of the cylinder calculated using Formula (1) is almost equal to that calculated using Formula (2). However, the critical buckling pressure of the cone calculated using Formula (1) is considerably smaller than that calculated using Formula (2), indicating that the cone on the inner side of the toroidal shell buckles first during hydroforming. As the hydroforming pressure continues to increase, the cylinder eventually buckles. According to previous studies [34,36,37], the failure modes of cylinders and cones under external pressure are represented as inward concave pits. Moreover, cones with imperfections in the study also exhibit the same failure mode [38,39]. Therefore, the failure modes of cylinders and cones can be regarded as wrinkling defects in toroidal shells during hydroforming.

**Table 3.** Critical buckling pressure calculated using analytical formulas.

	$p_{cr-cylinder}/\text{MPa}$	$p_{cr-cone}/\text{MPa}$
Formula (1)	3.380	0.256
Formula (2)	3.396	1.478

#### 4. Numerical Analysis

Because of the complex deformation that occurs during the hydroforming of toroidal shells, major discrepancies may be observed between analytical solutions obtained through theoretical calculations and the actual results. In this section, numerical methods are used to further analyze the hydroforming process of toroidal shells.

##### 4.1. Numerical Modeling

To investigate the hydroforming process of toroidal shells, the commercial software ABAQUS 2020 was used. The nonlinear analysis module in the software was used for the simulation. A three-dimensional preform model was established on the basis of the geometry depicted in Figure 1 and the geometric dimensions listed in Table 1. As shown in Figure 5, the model was imported into finite analysis software to mesh it and set its boundary conditions. To ensure the calculation accuracy and the quality of the elements, a four-node general-purpose shell element (S4) and a three-node triangular general-purpose shell element (S3) were used to partition the model. A grid convergence analysis was then conducted to evaluate the accuracy of the toroidal shell hydroforming process. Displace-

ment and stress were selected as convergence indicators. The size of the elements was successively reduced, and the number of elements was increased. As the mesh became finer, the displacement and stress results demonstrated a tendency to stabilize, indicating convergence. The determined element number was 17147 for the four-node element and 328 for the three-node element. In accordance with previous studies [31,40,41], a typical three-point boundary condition was selected as the constraint condition. This boundary condition has been effectively applied into various shells of revolution. The shell thickness was selected as an average thickness of 1.051 mm obtained through nondestructive measurement. The material properties were obtained from the average data provided in the last row of Table 2.

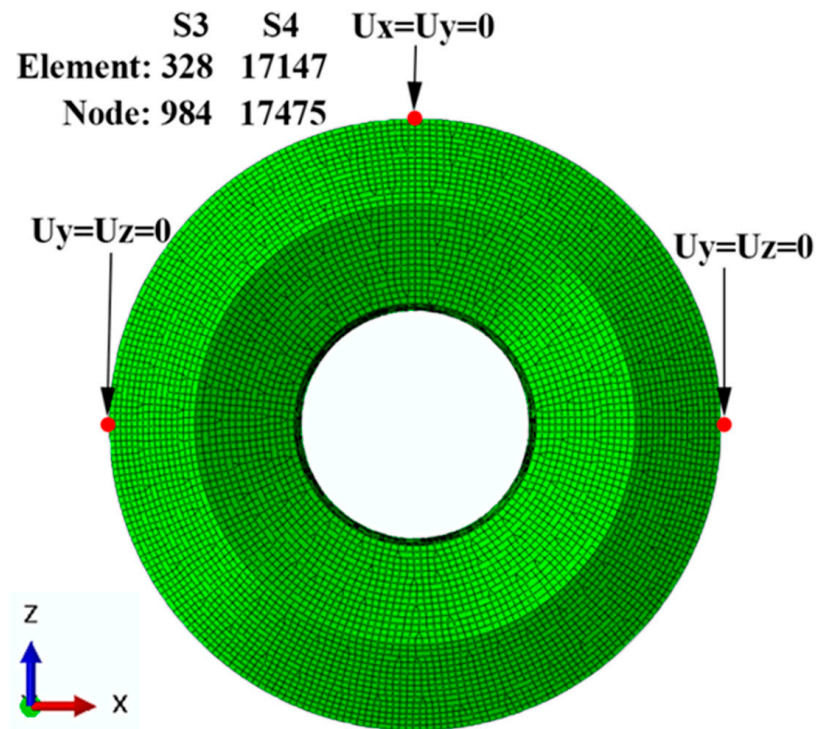


**Figure 5.** Finite element model of a toroidal preform with a hexagonal cross-section and a nominal geometry.

Two algorithms were used to simulate the hydroforming of a toroidal shell. The hydroforming process was evaluated using a general statics method. Internal pressures of 1.0, 1.5, 2.0, 2.5, 3.0, 3.5, 4.0, 4.5, 5.0, 5.5, and 6.0 MPa were directly applied to the model to simulate hydroforming. Subsequently, the internal pressure was reduced to 0 MPa to simulate springback. Consequently, a hydroformed shell state was obtained under various pressures. The algorithm settings for the general statistical method were as follows: an initial time increment of 0.1, a time period of 1, a minimum time increment of  $1 \times 10^{-50}$ , and a maximum time increment of 0.1. To determine the critical buckling pressures and identify the pressure at which wrinkling occurred in the toroidal shell, the Riks method was used. The algorithm settings for the Riks method were as follows: a maximum number of increments of 300, an initial increment of 0.01, a minimum arc length increment of  $1 \times 10^{-50}$ , and a maximum arc length increment of 0.01.

#### 4.2. Numerical Results and Discussion

During hydroforming, toroidal shells exhibit a gradual increase in the density of their wrinkles. Figure 6 shows numerical hydroformed models of an optimal toroidal preform with a hexagonal cross-section under different hydroforming pressures. At a hydroforming pressure of 1 MPa, small wrinkles appeared on the inner cone. When the hydroforming pressure reached 2 MPa, wrinkling occurred on the inner cylinder. These wrinkles manifested as a circle of independent protrusions. As the hydroforming pressure

further increased, large wrinkles started to split into smaller ones, which eventually merged. From a latitudinal viewpoint of the toroidal shell, the wrinkles on the inner cylinder were located exactly at the middle of two wrinkles on the inner cone. When the hydroforming pressure reached 4.5 MPa, the wrinkles on the internal cylinder became almost invisible. At a hydroforming pressure of 6 MPa, the wrinkles on the inner cone completely disappeared. These results indicate the ability of high hydroforming pressures to refine wrinkles. This refinement process is clearly depicted in Figure 6. In accordance with previous research [18], such wrinkles can be regarded as beneficial wrinkles that can be eliminated. However, excessive pressure may lead to toroidal shell cracking. In our simulation, we did not account for cracking. Therefore, the absence of wrinkles in our simulation does not guarantee their complete elimination in practical applications. Overall, the numerical results obtained using the general statics method agreed well with the analytical results. This agreement suggests that, during the hydroforming of toroidal shells, the inner cone tends to wrinkle before the inner cylinder does.

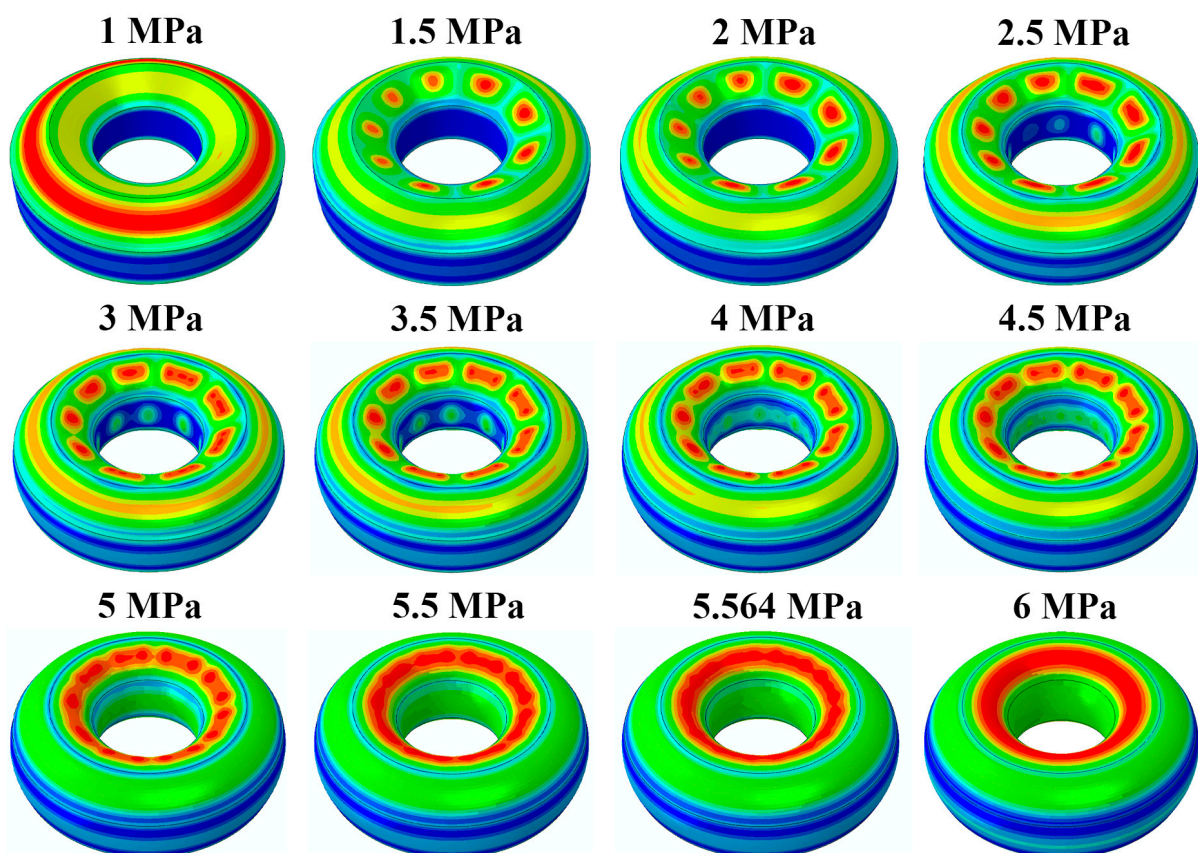


**Figure 6.** Numerical hydroformed models of an optimal toroidal preform with a hexagonal cross-section under different hydroforming pressures.

To determine the hydroforming state of the toroidal shell, a numerical model was placed under an experimental pressure of 5.564 MPa (Figure 6). At this moment, relatively small wrinkles were observed on the inner cone. Figure 7 presents the mechanical properties obtained under experimental pressure and after springback, including the equivalent stress, plastic strain, and wall thickness. Although these three physical quantities were uniformly distributed on the outer side of the toroidal shell in the circumferential direction, their distribution on the inner side of the toroidal shell was relatively complex, indicating the presence of both tensile stress and compressive stress on the inner side of the toroidal shell during the bulging process. Consequently, the distribution of stress and strain became uneven, leading to uneven changes in the wall thickness. These results verify the conjecture made in a previous analytical analysis.



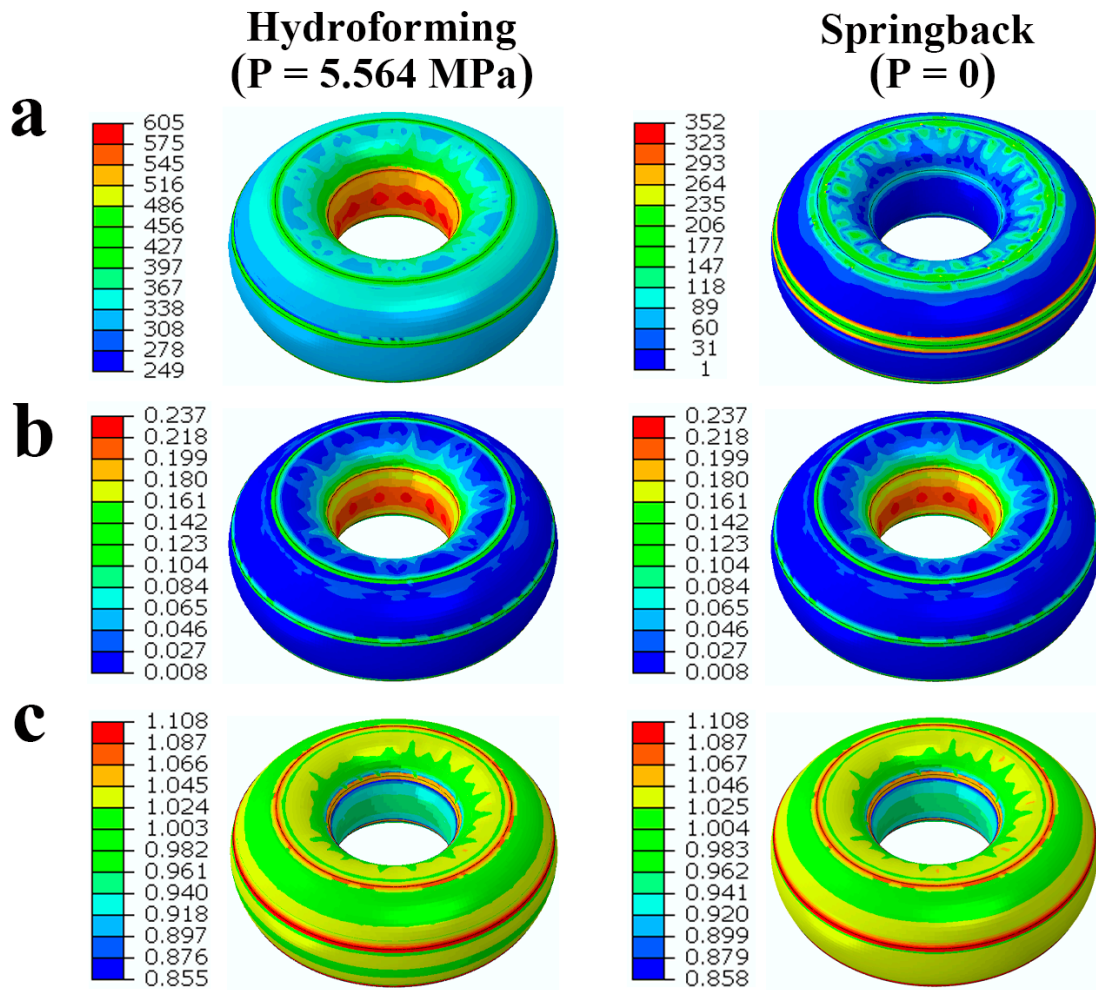


**Figure 7.** The obtained graphical results. (a) Equivalent stress, (b) plastic strain, and (c) wall thickness.

Figure 8 depicts a simulation of a pressure-arc length curve and deformation propagation during the hydroforming of a toroidal shell through the Riks method. At point P1, a pressure of 1.013 MPa was observed, corresponding to the wrinkling moment of the toroidal shell’s inner cone. This pressure was 295.7% higher than the critical buckling pressure of the inner cone calculated using Formula (1) but 45.9% lower than that calculated using Formula (2). At point P2, a pressure of 2.754 MPa was identified, corresponding to the wrinkling moment of the toroidal shell’s inner cylinder. This pressure was 22.7% lower than the critical buckling pressure of the inner cylinder calculated using Formula (1) and 23.3% lower than that calculated using Formula (2). Point P3 served as the critical buckling point of the toroidal shell under internal pressure. At this point, a pressure of 6.132 MPa was observed. At point P3, a sudden decrease in pressure occurred. Buckling under internal pressure also occurred throughout the entire toroidal shell. A comparison of the critical buckling pressures of the inner cone and inner cylinder calculated using the two formulas indicate that Formula (1) yielded the most conservative estimate. The numerical results also indicate that when the wrinkles on the inner cylinder were eliminated, the wrinkles on the inner cone were eliminated as well. These results suggest that the Riks method can be used to simulate the hydroforming of toroidal shells.



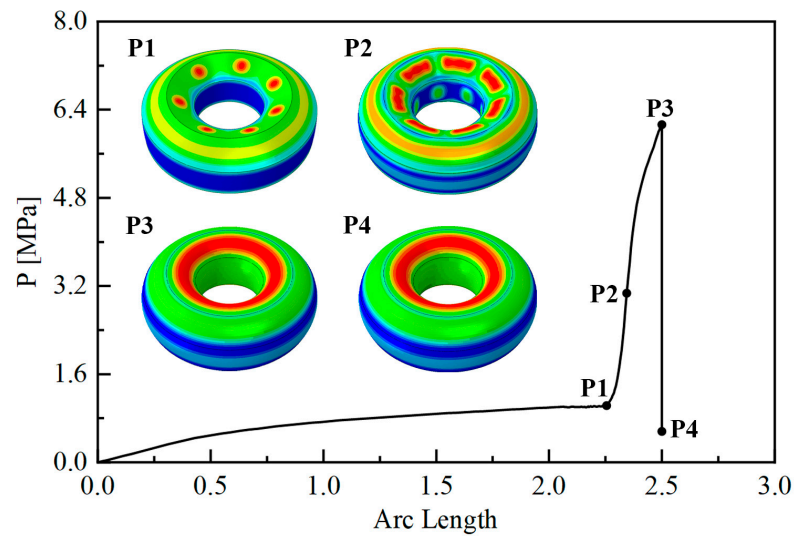


**Figure 8.** Simulation of a pressure-arc length curve and deformation propagation during the hydroforming of a toroidal shell through the Riks method.

### 5. Experimental Analysis

In this section, we discuss the methods used for the shape evaluation and toroidal preform hydroforming. Both the analytical and numerical results are benchmarked against experiments.

#### 5.1. Materials and Methods

Before hydroforming, a three-dimensional laser scanner (Open Technologies, Lombardy, Italy) with an error of less than 0.02 mm was used to scan the shape of the toroidal preform. Figure 9 shows the experimental settings of the optical geometric analysis. To enhance the contrast of the preform surface, a contrast enhancer was sprayed onto the preform to enable the improved differentiation of surface colors and features. Circular three-dimensional scanning marker points were attached to the surface of the toroidal preform to stitch the slices during scanning. Optical RevEng 2.3 software was used to process the scanning data and generate a complete geometric model. The scanned geometric model was used in a subsequent comparative analysis with an optimal model.

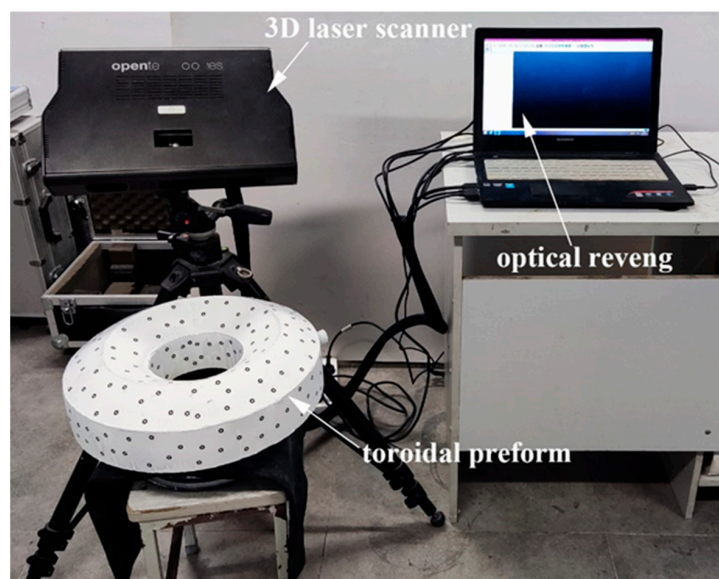


**Figure 9.** Experimental scene for optical geometry scanning.

During the hydroforming test, the toroidal preform was continuously injected with water to increase its internal pressure. Figure 10 shows a photograph of the toroidal shell hydroforming test. A manual pressure water pump with a maximum working pressure of 30 MPa and a maximum flow rate of 38 mL in a single stroke was used to inject water into the toroidal preform. A digital pressure sensor (SUP-P3000; United Test Automation, Hangzhou, China) with an error of less than 0.15 MPa and a maximum recorded pressure of 30 MPa was used to monitor pressure changes in the toroidal preform in real time. A data acquisition system (DH5902; Donghua Testing Technology, Jingjiang, China), whose sampling frequency was set to 50 Hz during the hydroforming test, was used to record changes in the internal pressure during the hydroforming process. The forming state of the shell was also continuously monitored. The internal pressure was gradually increased until the shell began to leak or reached the maximum pressure, at which point the test was halted.

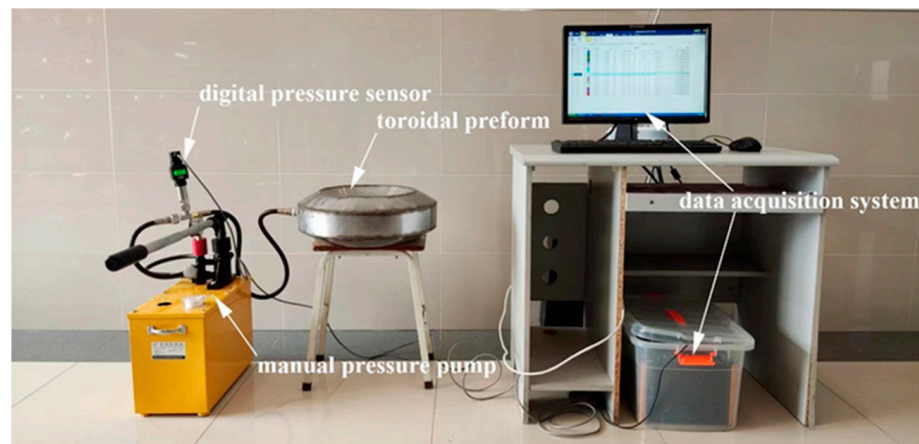


**Figure 10.** Photograph of the toroidal shell hydroforming test.

### 5.2. Experimental Results and Discussion

Overall, the toroidal preform exhibited a reasonable fabrication accuracy. Figure 11 shows the shape deviations of a toroidal preform with a hexagonal cross-section from an optimal corresponding geometry. In the figure, areas where the toroidal preform fit the optimal toroidal preform are represented in green. Most of the areas are green, indicating a favorable overall fit. According to the bar chart and distribution curve, shape deviations were concentrated near zero, indicating that the fabricated toroidal preform closely followed an optimal shape with minimal deviation. The maximum shape deviation was 3.00, and the minimum shape deviation was  $-1.50$ . These deviations occurred because of inaccurate splicing during assembly and thermal deformation during welding.

A final hydroforming pressure of 5.564 MPa was applied to the toroidal preform. Figure 12 presents the history of pressure applied in the hydroforming test. During the hydroforming of the toroidal preform, cracking and leakage were observed at the welding position under exposure to high internal pressure. However, this leakage was resolved by repair welding. Notably, the hydroforming test focused only on the hydroforming state of the toroidal shell and did not consider the welding residual stress caused by repair welding. Figure 12 shows the pressure of hydroforming after the last repair welding. When the hydroforming pressure reached 5.564 MPa, it exceeded the resistance capacity of the weld on the inner side of the toroidal shell. Consequently, a serious crack developed, resulting in an instantaneous decrease in the internal pressure of the toroidal shell to zero.

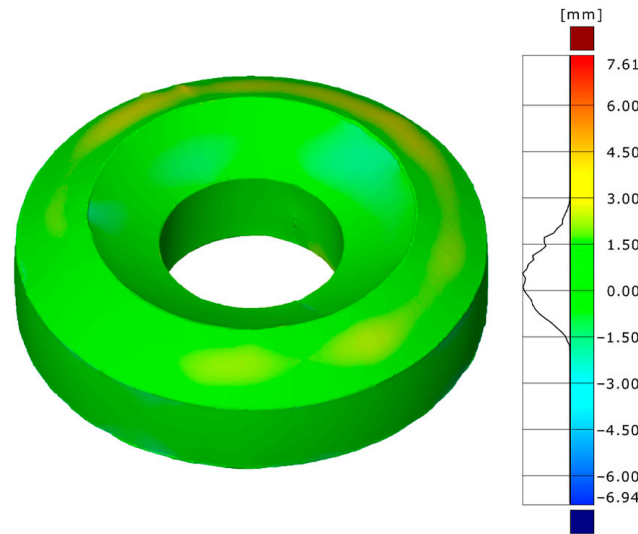


**Figure 11.** Shape deviations of a toroidal preform with a hexagonal cross-section from an optimal corresponding geometry.

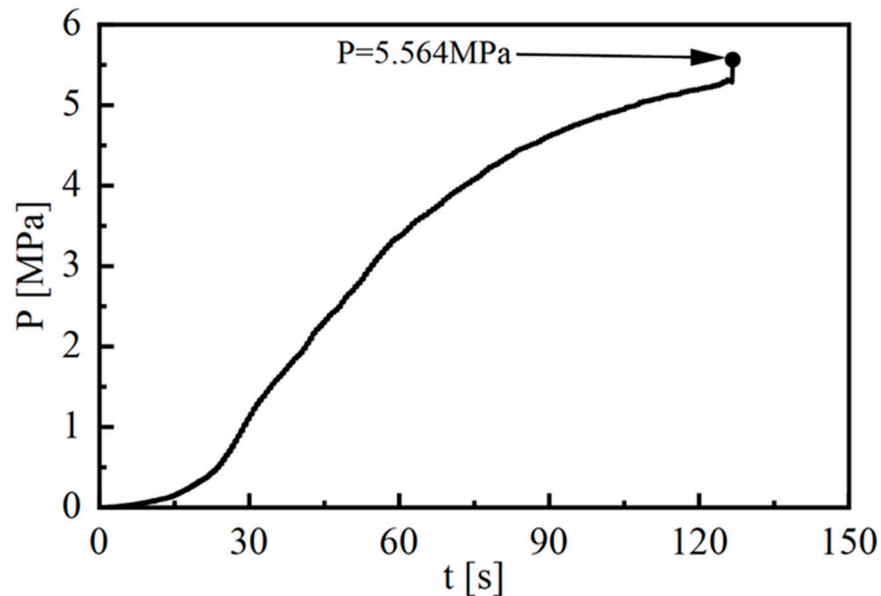


**Figure 12.** History of pressure applied in the hydroforming test.

Following the process of repair welding in the hydroforming test, multiple tests were conducted. Various scenarios were considered to determine the hydroforming state of the toroidal shell in the experiment. Due to the limitations of the experimental equipment, we are unable to observe even smaller wrinkles with the naked eye. Moreover, wrinkling is a rapid process, and we cannot instantly capture the state of wrinkling at a certain moment. These factors brought certain errors to our experimental results. Figure 13 shows a toroidal shell under different hydroforming pressures. The toroidal shell was actually a state within a relatively small range of corresponding pressures. With the exception of the toroidal shell in its initial and final states, the hydroforming and wrinkling states under various hydroforming pressures were recorded at intervals of 0.5 MPa. Before a hydroforming pressure of 5 MPa was reached, the number of wrinkles on the inner cone ranged from seven to eight. The number and shape of these wrinkles are consistent with the simulation results shown in Figures 6 and 8. The wrinkles on the inner cylinder are also identical to those depicted in Figures 6 and 8. As shown in Figure 13, the inner cone started to actually wrinkle after a hydroforming pressure of 1 MPa was reached, and the inner cylinder started



to wrinkle at a hydroforming pressure of 1.5 MPa. These results differ from those listed in Table 3, indicating that analytical calculations provide conservative predictions. Thus, Formula (1) was deemed to be more conservative than Formula (2) in terms of predicting the buckling value of cones.

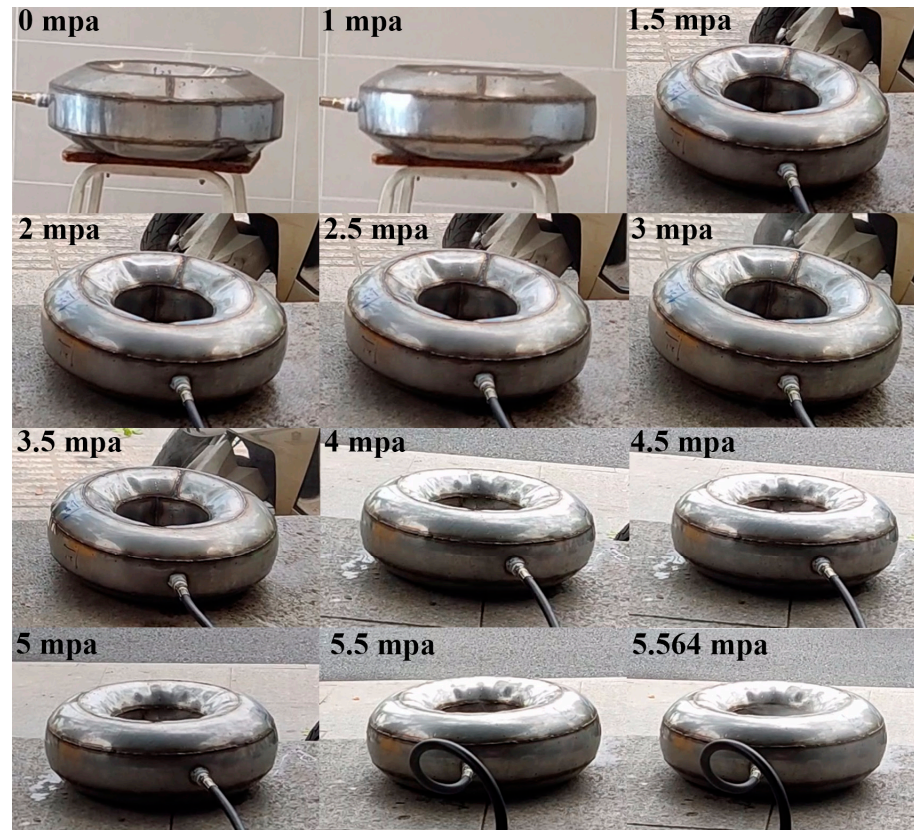


**Figure 13.** A toroidal shell under different hydroforming pressures.

When the hydroforming pressure reached 5.564 MPa, both large and small wrinkles remained. Figure 14 shows the hydroformed toroidal shell and the wrinkling area. This state is consistent with the wrinkling state depicted in Figure 6. Before refinement and densification, the number of wrinkles primarily ranged from seven to eight. As the pressure increased, the number of wrinkles increased exponentially. Although the wrinkles on the inner cone and cylinder were already dense, they did not reach the elimination level (Figure 14). Therefore, the hydroforming pressure did not increase. Thus, the wrinkles observed on the inner cylinder and cone of the toroidal preform were regarded as dead wrinkles that could not be eliminated.

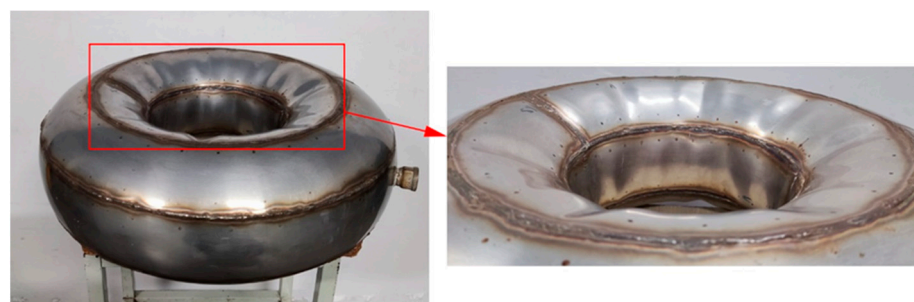


**Figure 14.** The hydroformed toroidal shell and wrinkling area.

## 6. Optimization of the Preform Geometry

In accordance with the aforementioned assessment of the reasons underlying wrinkling, as described in this section, we modified the initial structure of the toroidal preform and evaluated the effect of the preform geometry by conducting analytical calculations and numerical simulations.

### 6.1. Design of the Geometric Structure

Previous studies have indicated that increasing the number of segments on the inner side of a toroidal preformed structure may help to avoid wrinkling [29,30]. In accordance with these studies, we attempted to improve our initial preform structure (Figure 1). Based on the findings from the preceding sections of research, it was observed that wrinkles manifest in the toroidal shell characterized by a negative Gaussian curvature during the hydroforming process. Conversely, the segments featuring a positive Gaussian curvature and zero Gaussian curvature within the toroidal shell undergo normal formation. Therefore, for the optimization of preform geometry, we made changes to the structure of the negative Gaussian curvature part of the toroidal preform with a hexagonal cross-section. Figure 15 depicts the geometry of the improved toroidal preform. To regulate the variable parameters in the study, the geometric properties of the toroidal preform, such as its rotating radius, uniform thickness, and target toroidal shell cross-sectional radius, remained unchanged. The outer structure of the improved toroidal preform also remained unchanged. However, the three original inner segments were increased to four segments of equal length. The length of Segment A was 75 mm, and the length of Segment B was 57.4 mm.

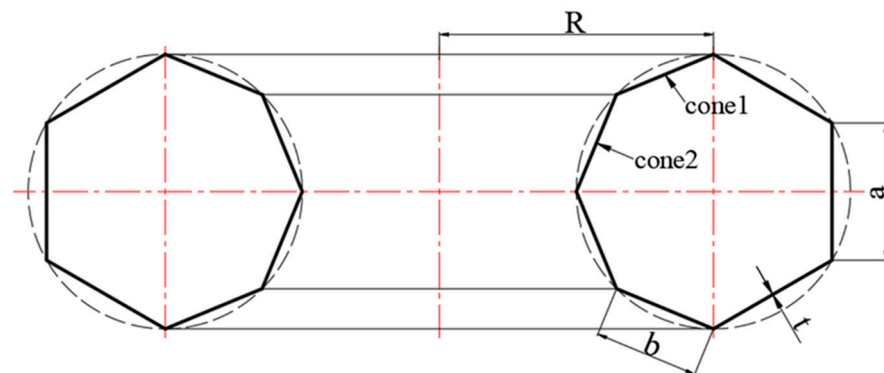


**Figure 15.** Geometry of a toroidal preform with an improved cross-section.

### 6.2. Results and Discussion

Both analytical and numerical techniques were used to evaluate the improved toroidal preform. The results indicate that the material properties were consistent with the original structure analysis. Formulas (1) and (2) were used to calculate the critical buckling pressure of the inner shell. As shown in Table 4, the results indicate that the closer the segment was to the outer cone, the lower the critical buckling pressure was. These results confirm that the outer side of the toroidal preform was easily deformable. To predict wrinkling during hydroforming, Formulas (1) and (2) were compared in terms of their conservative prediction capabilities. Formula (1) was ultimately selected to predict the occurrence of wrinkling. When this formula was used, Cone 1 was predicted to experience wrinkling at a pressure of 0.41 MPa, whereas Cone 2 was predicted to reach the wrinkling threshold at a pressure of 2.98 MPa. According to the analytical results for an unmodified toroidal shell, Formula (1) provided a conservative estimate. In addition, the critical buckling pressure in the inner cone of the modified toroidal shell was higher than that in the previous shell, indicating the low likelihood of wrinkling in the modified toroidal shell.

**Table 4.** Critical buckling pressure in the inner shell after structural modification.

	$p_{cr-cone1}/\text{MPa}$	$p_{cr-cone2}/\text{MPa}$
Formula (1)	0.51	2.98
Formula (2)	1.62	4.22

To accurately determine the wrinkling state during hydroforming, a numerical hydroforming process diagram similar to that depicted in Figure 6 was established, as shown in Figure 16. At a hydroforming pressure of 1.5 MPa, wrinkles appeared on Cone 1 but not on Cone 2. However, when the bulging pressure reached 4 MPa, all wrinkles on the hydroformed toroidal shell completely disappeared. Compared with the toroidal preform without an improved initial structure, the wrinkles of the improved toroidal preform were less obvious. In addition, the hydroforming pressure decreased when the wrinkles disappeared, indicating that the wrinkles observed during hydroforming were beneficial wrinkles that could be eliminated through the application of a high internal pressure. This finding suggests that increasing the number of segments on the inner side of a toroidal preform to improve its structure may help to eliminate wrinkles and improve the overall hydroforming quality of toroidal shells.

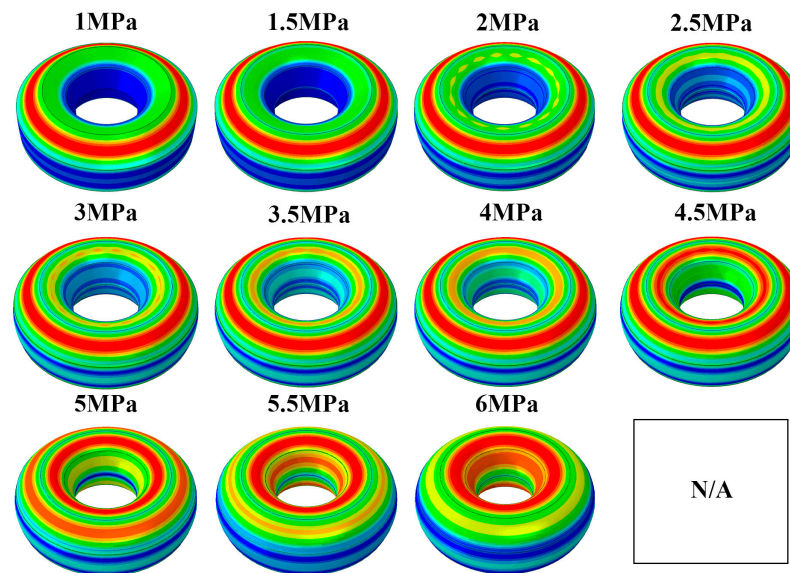


**Figure 16.** Numerical hydroformed models of an optimal toroidal preform with an improved cross-section under various hydroforming pressures.

### 7. Conclusions

In this study, we conducted analytical, numerical, and experimental analyses of the wrinkling phenomenon of toroidal preforms during hydroforming and proposed a method for eliminating wrinkling. The following points are the main conclusions of this study:

- (1) The theoretically derived analytical solution for toroidal shell wrinkling during hydroforming demonstrated a conservative nature. When wrinkles appeared on the inner cone, a substantial variation of approximately 295.7% was obvious between the pressure calculated using Kollar’s proposed formula and the numerical estimation results. Conversely, a relatively smaller difference of approximately 22.7% was observed between the numerical evaluation outcomes and the wrinkling estimation results of the inner cylinder of the toroidal shell. The analytical solution exhibited a conservative predictive tendency for both identifying the shell element that wrinkles and estimating the hydroforming pressure during wrinkling.



- (2) Wrinkling occurs during hydroforming in the inner region of toroidal shells. Employing both general statics and Riks methods was proven to be effective and feasible for simulating the hydroforming process of toroidal shells.
- (3) The wrinkling state observed during the experiment agreed well with the numerical simulation results. Before a finer and denser state was reached, the number of folds primarily ranged from seven to eight. As the pressure continued to increase, the number of observed wrinkles increased exponentially.
- (4) By increasing the number of segments on the inner side of the toroidal preform, wrinkles can be effectively eliminated. Having an increased number of segments on the inner side contributed significantly to the enhancement of the structural integrity and resistance to wrinkling under the influence of raised internal pressures.

Notably, we did not consider the welding effect of toroidal preforms in the current analysis, and we did not measure the distribution of stress during the experiment. These factors may affect the conditions of wrinkling. Therefore, further analysis is required to investigate the effects of welding stress and experimental conditions on the occurrence of wrinkling. Further research is also required to examine and refine the analytical formula of toroidal shells in order to increase the accuracy of the mathematical models used.

**Author Contributions:** Conceptualization, X.L. and J.Z.; methodology, X.L., W.W. and J.Z.; software, X.L.; validation, M.Z. and X.Z.; investigation, X.L. and K.X.; data curation, X.L.; writing—original draft preparation, X.L.; writing—review and editing, J.Z. and M.Z.; visualization, M.Z. and X.Z.; supervision, X.Z. and W.W.; funding acquisition, J.Z.; formal analysis, M.Z. and K.X. All authors have read and agreed to the published version of the manuscript.

**Funding:** This work was supported by the National Natural Science Foundation of China (Grant Number 52071160), Outstanding Youth Foundation of the Jiangsu Scientific Committee (Grant Number BK20230014).

**Institutional Review Board Statement:** Not applicable.

**Informed Consent Statement:** Not applicable.

**Data Availability Statement:** All data are included in the manuscript.

**Conflicts of Interest:** The authors declare no conflicts of interest.

## References

1. Wang, Z.R. *Shell and Tube Hydroforming: Mechanics of Dieless Closed Shell Hydro-Bulging*; Higher Education Press: Beijing, China, 2018; pp. 343–364.
2. Wang, Z.R.; Yuan, S.J.; Teng, B.G. *Theory and Key Techniques of Hydro-bulging Spherical Vessels*, 1st ed.; Harbin Institute of Technology Press: Harbin, China, 2014; pp. 141–154.
3. Yuan, S.J. *Modern Hydroforming Technology*, 2nd ed.; National Defence Industry Press: Beijing, China, 2016; pp. 267–313.
4. Zhang, R.; Zhang, W.W.; Yuan, S.J. Research on Hydro-Forming of Spherical Shells with Different Preform Types. *Int. J. Adv. Manuf. Technol.* **2017**, *92*, 2631–2638. [[CrossRef](#)]
5. Jing, Y.; Guan, J.; Kong, C.; Zhao, W.; Gomi, N.; Zhao, X. Integral Bulge Forming Method for Soccer Ball-Shaped Tank Using Symmetrical Preformed Box Consisting of Plate Parts. *Am. J. Mech. Appl.* **2022**, *10*, 16–24. [[CrossRef](#)]
6. Zhang, S.H.; Jiang, L.; Wang, B.L.; Wang, Z.R. Finite-Element Analysis of the Integral Hydrobulge Forming of Double-Layer Gap Spherical Vessels. *Int. J. Press. Vessel. Pip.* **1996**, *68*, 161–167. [[CrossRef](#)]
7. Zhang, W.W.; Teng, B.G.; Yuan, S.J. Research on Deformation and Stress in Hydroforming Process of an Ellipsoidal Shell without Constraint. *Int. J. Adv. Manuf. Technol.* **2015**, *76*, 1555–1562. [[CrossRef](#)]
8. Zeng, Y.S.; Wang, Z.R.; Yuan, S.J. The Numerical Simulation of the Integral Hydrobulging of Ellipsoidal Shells. *J. Mater. Process. Technol.* **1997**, *72*, 358–362. [[CrossRef](#)]
9. Alves, L.M.; Martins, P.A.F. Forming of Thin-Walled Tubes into Toroidal Shells. *J. Mater. Process. Technol.* **2010**, *210*, 689–695. [[CrossRef](#)]
10. Yuan, S.J.; Xu, Z.; Wang, Z.R.; Hai, W. The Integrally Hydro-Forming Process of Pipe Elbows. *Int. J. Press. Vessel. Pip.* **1998**, *75*, 7–9. [[CrossRef](#)]
11. Liu, N.; Yang, H.; Li, H.; Yan, S. Plastic Wrinkling Prediction in Thin-Walled Part Forming Process: A Review. *Chin. J. Aeronaut.* **2016**, *29*, 1–14. [[CrossRef](#)]

12. Sun, B.H. Geometry-Induced Rigidity in Elastic Torus from Circular to Oblique Elliptic Cross-Section. *Int. J. Non-Linear Mech.* **2021**, *135*, 103754. [[CrossRef](#)]
13. Sun, B.H. Gol'denveizer's Problem of Elastic Torus. *Thin-Walled Struct.* **2022**, *171*, 108718. [[CrossRef](#)]
14. Lubis, A.; Su'Udi, A. Ring Stability of Underground Toroidal Tanks. *AIP Conf. Proc.* **2017**, *1855*, 040003. [[CrossRef](#)]
15. Pietraszkiewicz, W.; Konopińska, V. Junctions in Shell Structures: A Review. *Thin-Walled Struct.* **2015**, *95*, 310–334. [[CrossRef](#)]
16. Du, Q.; Cui, W.; Zhang, B. Buckling Characteristics of a Circular Toroidal Shell with Stiffened Ribs. *Ocean Eng.* **2015**, *108*, 325–335. [[CrossRef](#)]
17. Zhang, S.H.; Zhang, Y.S.; Wang, Z.R.; Yuan, S.J.; Wang, F.C.; Liu, C.Q. The Integral Hydro-Bulge Forming of Oblate Spheroidal Shells. *J. Plast. Eng.* **1995**, *2*, 26–35.
18. Yuan, S.J.; Wang, X.S. Fundamentals and Application of Tube Hydro-Forming. *Chin. J. Mech. Eng.* **2002**, *38*, 12–15. [[CrossRef](#)]
19. Yuan, S.; Gai, B. Variational Principle of Plastic Buckling of Plates. *J. Plast. Eng.* **2004**, *11*, 12–15.
20. Liu, W.; Xu, Y.; Yuan, S. Effect of Pre-Bulging on Wrinkling of Curved Surface Part by Hydromechanical Deep Drawing. *Procedia Eng.* **2014**, *81*, 914–920. [[CrossRef](#)]
21. Liu, W.; Chen, Y.Z.; Xu, Y.C.; Yuan, S.J. Enhancement on Plastic Deformation of Curved Surface Shell by Sheet Hydroforming with Optimized Pre-Bulging Process. *Int. J. Adv. Manuf. Technol.* **2018**, *97*, 4145–4156. [[CrossRef](#)]
22. Chen, Y.Z.; Liu, W.; Xu, Y.C.; Yuan, S.J. Analysis and Experiment on Wrinkling Suppression for Hydroforming of Curved Surface Shell. *Int. J. Mech. Sci.* **2015**, *104*, 112–125. [[CrossRef](#)]
23. Chen, Y.Z.; Liu, W.; Zhang, Z.C.; Xu, Y.C.; Yuan, S.J. Analysis of Wrinkling during Sheet Hydroforming of Curved Surface Shell Considering Reverse Bulging Effect. *Int. J. Mech. Sci.* **2017**, *120*, 70–80. [[CrossRef](#)]
24. Rezaiee-Pajand, M.; Masoodi, A.R. Shell Instability Analysis by Using Mixed Interpolation. *J. Braz. Soc. Mech. Sci. Eng.* **2019**, *41*, 419. [[CrossRef](#)]
25. Rezaiee-Pajand, M.; Masoodi, A.R. Analyzing FG Shells with Large Deformations and Finite Rotations. *World J. Eng.* **2019**, *16*, 636–647. [[CrossRef](#)]
26. Rezaiee-Pajand, M.; Masoodi, A.R.; Arabi, E. A 6-Parameter Triangular Flat Shell Element for Nonlinear Analysis. *Eur. J. Comput. Mech.* **2019**, *28*, 237–268. [[CrossRef](#)]
27. Kawka, M.; Olejnik, L.; Rosochowski, A.; Sunaga, H.; Makinouchi, A. Simulation of Wrinkling in Sheet Metal Forming. *J. Mater. Process. Technol.* **2001**, *109*, 283–289. [[CrossRef](#)]
28. Yuan, S.J.; Wang, Z.R.; He, Q. Finite Element Analysis of Hydro-Forming Process of a Toroidal Shell. *Int. J. Mach. Tools Manuf.* **1999**, *39*, 1439–1450. [[CrossRef](#)]
29. Teng, B.G.; Yuan, S.J.; Wang, Z.R. Effect of the Initial Structure on the Hydro-Forming of Toroidal Shells. *J. Mater. Process. Technol.* **2002**, *123*, 18–21. [[CrossRef](#)]
30. Teng, B.G.; Yuan, S.J.; Wang, Z.R. Experiment and Numerical Simulation of Hydro-Forming Toroidal Shells with Different Initial Structure. *Int. J. Press. Vessel. Pip.* **2001**, *78*, 31–34. [[CrossRef](#)]
31. Zhang, J.; Liu, X.; Zhan, M.; Wang, F.; Zhao, X. Hydroforming and Buckling of Toroids with Polyhedral Sections. *Ships Offshore Struct.* **2022**, *18*, 937–947. [[CrossRef](#)]
32. Ventsel, E.; Krauthammer, T. *Thin Plates and Shells: Theory, Analysis, and Applications*; CRC Press: New York, NY, USA, 2001.
33. Tang, W.; Li, S.; Zhang, J.; Wang, Y.; Wang, W.; Zhang, S. Numerical and Experimental Study on Buckling of Longitudinal Corrugated Cylindrical Pressure Shell. *J. Mech. Eng.* **2020**, *56*, 164–170. [[CrossRef](#)]
34. Zhang, J.; Zhang, S.; Cui, W.; Zhao, X.; Tang, W.; Wang, F. Buckling of Circumferentially Corrugated Cylindrical Shells under Uniform External Pressure. *Ships Offshore Struct.* **2019**, *14*, 879–889. [[CrossRef](#)]
35. Zhang, J.; Zhu, Z.; Wang, F.; Zhao, X.; Zhu, Y. Buckling Behaviour of Double-Layer and Single-Layer Stainless Steel Cylinders under External Pressure. *Thin-Walled Struct.* **2021**, *161*, 107485. [[CrossRef](#)]
36. Zingoni, A.; Enoma, N. Strength and Stability of Spherical-Conical Shell Assemblies under External Hydrostatic Pressure. *Thin-Walled Struct.* **2020**, *146*, 106472. [[CrossRef](#)]
37. Ross, C.T.F. Collapse of Corrugated Circular Cylinders Under Uniform External Pressure. *Int. J. Struct. Stab. Dyn.* **2005**, *17*, 241–257. [[CrossRef](#)]
38. Ghazijahani, T.G.; Showkati, H. Experiments on Conical Shell Reducers under Uniform External Pressure. *J. Constr. Steel Res.* **2011**, *67*, 1506–1515. [[CrossRef](#)]
39. Ghazijahani, T.G.; Showkati, H. Locally Imperfect Conical Shells Under Uniform External Pressure. *Strength Mater.* **2013**, *45*, 157–168. [[CrossRef](#)]
40. Błachut, J. Buckling and First Ply Failure of Composite Toroidal Pressure Hull. *Comput. Struct.* **2004**, *82*, 1981–1992. [[CrossRef](#)]
41. Zhang, J.; Wang, X.; Tang, W.; Wang, F.; Zhu, Y. Non-Linear Collapse Behavior of Externally Pressurized Resin Toroidal and Cylindrical Shells: Numerical and Experimental Studies. *Ships Offshore Struct.* **2021**, *16*, 529–545. [[CrossRef](#)]

**Disclaimer/Publisher's Note:** The statements, opinions and data contained in all publications are solely those of the individual author(s) and contributor(s) and not of MDPI and/or the editor(s). MDPI and/or the editor(s) disclaim responsibility for any injury to people or property resulting from any ideas, methods, instructions or products referred to in the content.